Near infrared quantum cutting of Na$^+$ and Eu^{2+}-Yb^{3+} couple activated SrF$_2$ crystal

M.Y.A. Yagoub [a], H.C. Swart [a], M.S. Dhlamini [b], E. Coetsee [a, *]

[a] Department of Physics, University of the Free State, P.O. Box 339, Bloemfontein, ZA9300, South Africa
[b] Department of Physics, University of South Africa, P.O. Box 392, Pretoria, ZA0003, South Africa

ARTICLE INFO

ABSTRACT

Na$^+$ and Eu^{2+}-Yb^{3+} couple activated SrF$_2$ phosphor powders were synthesized by the co-precipitation method. The structure and luminescence properties of the system were investigated. X-ray diffraction data indicated that a mixture of cubic SrF$_2$ and NaYbF$_4$ phases gradually formed with an increase in the Yb^{3+} ion doping concentration. Diffuse reflectance has been used to confirm the existence of europium in the divalent state. The possibility of quantum cutting in the Eu^{2+}–Yb^{3+} ions co-doped SrF$_2$ crystal was discussed. Energy transfer that occurred subsequently from Eu^{2+} to Yb^{3+} was followed by an intense near-infrared (NIR) (~1000 nm) emission spectral range. Emission spectra and the fluorescence decay measurements have been utilized to demonstrate the cooperative energy transfer in the Eu^{2+}-Yb^{3+} couple ions. The energy transfer was completed at high concentration and the Yb^{3+} ions emission's intensity was reduced as a result of concentration quenching. In addition from the photoluminescence data it was also evident that Na$^+$ induced a significant change to the NIR emission.

© 2016 Elsevier B.V. All rights reserved.

1. Introduction

The major problem for low theoretical quantum efficiency of crystalline Silicon (c-Si) solar cells is related to the Shockley-Queisser limit. This is due to the spectral mismatch between the c-Si and the incident photons. Recent studies of solar mismatch modification are mostly devoted to up-conversion and down-conversion materials [1,2]. Up-conversion is where two lower energy photons (lower than c-Si) are added to generate one higher energy photon that can be used in the solar cell conversion. Up-conversion is a nonlinear process which requires a high-excitation density to achieve high conversion efficiency. Down-conversion is a linear process and a high-excitation density is not a requirement [1]. Down-conversion (quantum cutting) is a process where one UV/visible photon split into two near-infrared (NIR) photons where the spectral response of the solar cell is high [1–4]. Both these photons can then be absorbed by the solar cell. The down-conversion gives rise to an additional advantage that minimize the energy loss due to thermalization of hot charge carriers after absorption of high energy photons. Most of the down-conversion studied materials are based on the energy transfer from lanthanide ions to the Yb^{3+} ion [2]. This is because Yb^{3+} has a single excited state (^{2}F$_{5/2}$) approximately 10000 cm^{-1} above the ^{2}F$_{7/2}$ ground state. The absence of the energy levels above the excited state (^{2}F$_{5/2}$) allows Yb^{3+} to absorb energy packages of 10000 cm^{-1} from other co-doped lanthanide ions and emits photons around ~1000 nm where silicon solar cells shows high spectral response. Down-conversion has been investigated in various rare earth couples (Ln^{3+}–Yb^{3+} (Ln = Pr, Er, Nd, Ho, Dy, Tb and Tm) in different hosts in which the Ln^{3+} ions act as the absorption centers [2,5,6]. Absorption of photons by these ions results in feeding two Yb^{3+} ions, which turns out to emit two near infrared photons that can be used for creating two electron-hole pairs. Ideal NIR down-converting materials for c-Si solar cells should efficiently convert the UV/Vis broadband part of the solar spectrum into ~1000 nm NIR photons. However, the low absorption cross-section (typically on the order of 10^{-21} cm^2) of the 4f-4f transition of the down-converting materials based on the Ln^{3+}–Yb^{3+} couples, limit the implementation of such application [1]. On the contrary, the dipole-allowed 4f–5d have stronger absorption cross-sections of up to 10^{-18} cm^2. Recently much attention have been paid to the broadband NIR down-conversion through Ce^{3+}, Eu^{2+} and Yb^{2+} ions that sensitize both the Yb^{3+} or Ln^{3+}–Yb^{3+} ion couples [1,7–10]. The 4f-5d broadband ions' transitions strongly

depend on the crystal field of the host to utilize sensitization through direct cooperative energy transfer from the broadband ions to Yb^{3+}. In our previous investigation of the energy transfer between Eu^{2+} and Pr^{3+} co-doped SrF_2, we demonstrated excellent sensitization effects of the Eu^{2+} ion on the luminescence properties of the Pr^{3+} ion [11]. The luminescence intensities of the Pr^{3+} ion were greatly enhanced with the co-doping of Eu^{2+} ions. Furthermore, the 5d level of the Eu^{2+} ion was found to emit blue photons centred at 416 nm [11,12], which is approximately twice that of the Yb^{3+} emission in SrF_2.

The SrF_2 crystal is one of the widely used hosts in various applications [13–16]. The photoluminescence (PL) properties of SrF_2 doped by Ln^{3+} ions have been extensively investigated in which charge compensation for the substitution of Ln^{3+} for Sr^{2+} is required. This gives rise to a rich multisite structure, which leads to broad absorption and emission bands. The disadvantage of such charge compensation (fluorine interstitial) is that it would reduce the quantum efficiency of the system [17]. A new class of charge compensation that is based on monovalent impurity ions that exist along with the Ln^{3+} ions into the fluorite hosts have been reported [17–20]. Co-doping Yb^{3+} with Na^+ as a charge compensator decreases the multisites of Yb^{3+} since Yb^{3+}–Na^+ complexes are expected to dominate the system [17]. In this work, the influence of the Na^+ ions on the photoluminescence of SrF_2:Eu^{2+}, Yb^{3+} is studied for possible down-conversion application in solar cells. The cooperative energy transfer process from Eu^{2+} to Yb^{3+} ions is also discussed.

2. Experimental

For the co-precipitation process, analytical grade of $Sr(NO_3)_2$, $Eu(NO_3)_3 \cdot 5H_2O$, $Yb(NO_3)_3 \cdot 5H_2O$, NaOH and NH_4F were used without further purification. For a typical synthesis of SrF_2:Eu^{2+},Yb^{3+}, 30 mmol of NH_4F and 0.1 mol/mL of NaOH were added drop-wise to an aqueous solution containing $Sr(NO_3)_2$, $Yb(NO_3)_3 \cdot 5H_2O$ and $Eu(NO_3)_3 \cdot 5H_2O$ in periods of about 30 min. After 1 h of stirring, the mixture was left for 5 h. Then the product was collected by using a centrifugal and washed with water and ethanol. Finally, the product was dried for 48 h in an oven at 80 °C. The samples were annealed under a reducing atmosphere (Ar 96%/H_2 4%) in order to reduce Eu^{3+} into Eu^{2+} ions.

The structure of the prepared samples was characterised by X-ray diffraction (XRD) using a Bruker Advance D8 diffractometer (40 kV, 40 mA) with Cu K_α x-rays ($\lambda = 0.154$ nm). UV–Vis–NIR diffuse reflection spectra were measured using a Perkin Elmer Lambda 950 spectrophotometer with an integrating sphere and using spectralon as the reference material. Photoluminescence spectra (PL) were collected by using a Cary Eclipse fluorescence spectrophotometer equipped with a xenon lamp. The NIR PL spectra were collected with a He–Cd laser PL system with a 325 nm excitation wavelength and a 2 mm InGaAs photodiode detector. Luminescence decay curves of Eu^{2+} were recorded under pulsed excitation (HORIBA scientific) with a 375LH NanoLED diode with a 375 nm excitation wavelength. All measurements were performed at room temperature.

3. Results and discussion

It is worth mentioning that the Na^+ concentration was fixed to 0.5 mol% throughout this study. Fig. 1 shows the XRD patterns of singly doped Eu^{2+} and co-doped Eu^{2+}-Yb^{3+} ions in the SrF_2 crystal. For Eu^{2+} singly doped SrF_2, the pattern crystallized into the cubic structure of SrF_2 (card 00-086-2418). Co-doping with low concentrations of Yb^{3+} ions (up to 3 mol%) with the Na^+ ion in the SrF_2:Eu^{2+} (1.5 mol%) structure did not cause any change in the XRD

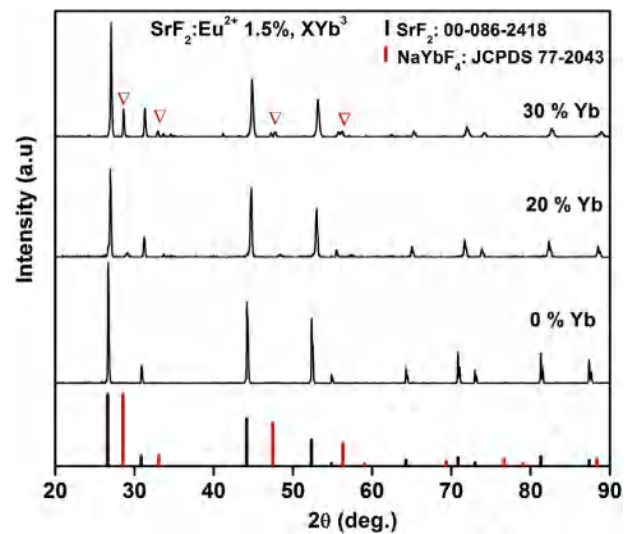**Fig. 1.** XRD patterns of the SrF_2:Eu^{2+}(1.5 mol%) crystals and a mixture of the SrF_2 and $NaYbF_4$ XRD patterns obtained after co-doping with high Yb^{3+} concentration and 0.5 mol% Na. The peaks marked with a triangle refer to the cubic-phase of $NaYbF_4$. The SrF_2 and $NaYbF_4$ standard XRD patterns are also shown.

patterns. With increased Yb^{3+} ions' concentration, the XRD patterns of the samples can be indexed as a mixture of the cubic phases for SrF_2 and $NaYbF_4$ (JCPDS 77-2043). The schematic structure of pure SrF_2 is shown in Fig. 2(A). The Sr^{2+} sub-lattice is face-centred cubic, the F^- sub-lattice is simple cubic where each second cube contains Sr^{2+} ions (the others are empty). The divalent (Eu^{2+}) ion easily substitutes for the central Sr^{2+} ion, leaving it in a crystalline environment. In general, when Yb^{3+} ions are co-doped in the system, the extra positive charge of the Yb^{3+} relative to the Sr^{2+} ion
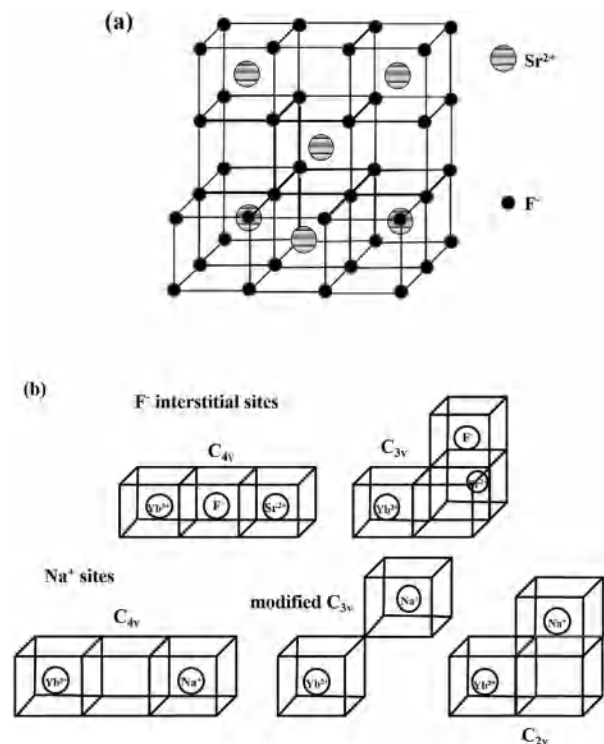

Fig. 2. (a) A pure SrF_2 structure showing that every second simple cubic of the F^- sub-lattice contains a Sr^{2+} ion. (b) Schematic pictures of some Yb^{3+} ions' charge compensation pairs (i.e. both the Na sub-situational sites and the F interstitial sites).

makes some type of charge-compensation mechanism necessary, which is required to maintain the electrical neutrality of the crystal. The O_h (cubic) symmetry of the Sr^{2+} site would changed to the lower symmetries, tetragonal (C_{4v}) and trigonal (C_{3v}), respectively [17,22]. Fig. 2(b) shows the possible F^- interstitial sites. Co-doping with Yb^{3+} and Na^+ ions in the SrF_2 crystals can also cause the Na^+ ions to compensate with the extra charge of the Yb^{3+} ion. The Na^+ ions can therefore enter in sub-substitution or interstitial positions near the Yb^{3+} ions and then result in a modified C_{3v} symmetry (Fig. 2(B)) [19]. Some of the possible sites for Na^+ ions in the SrF_2 host are shown in Fig. 2(B). The cubic $NaYbF_4$ system is a fluorite structure (SrF_2) with the Sr^{2+} sites randomly occupied by Na^+ and Yb^{3+} ions [21]. Thus, the presence of Na^+ ions with increased Yb^{3+} concentration in the SrF_2 structure gradually leads to the formation of a mixed cubic structure between SrF_2 and $NaYbF_4$.

Fig. 3 depicts the diffuse reflectance spectra of 1.5 mol% Eu^{2+} co-doped with 15 and 30 mol% Yb^{3+} concentration in the SrF_2: Na^+ (0.5 mol%) to confirm the existence of europium in the divalent state. The broad absorption band located between 275 and 400 nm is a result of the strong absorption of the Eu^{2+} ($4f^7$-$4f^65d$) ion. It can be seen that the absorption strengths for the peaks corresponding to Eu^{2+} ions have similar absorption strength for the two samples, which demonstrates that the Eu^{2+} is equally incorporated in the SrF_2 crystal. The absorption peak in the NIR part with a maxima at 976 nm is assigned to the 4f-4f transition of the Yb^{3+} ion. The weak sensitivity of our system in the NIR region results in a weak and noisy intensity signal for the low Yb^{3+} concentration. As expected, the intensity of the NIR absorption band increased with increasing Yb^{3+} doping concentration. It is well known that the interstitial fluorine sites induce broad excitation bands to trivalent rare-earth ions-doped SrF_2 due to a rich multisite structure of several types of charge compensation (nearest neighbor (C_{4v}), next nearest neighbor (C_{3v}) or no local site (O_h) and various clusters) [17,22]. If Na^+ ions are also present in fluoride host it leads to narrow absorption and emission bands of the Ln^{3+} ions [18]. Due to the weak sensitivity of our UV–vis system in the NIR region no significant change has been observed in the NIR absorption spectra for both the F^- and Na^+ sites.

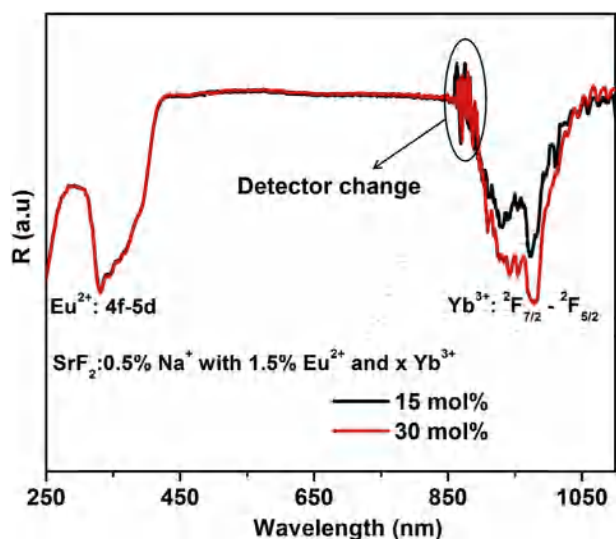The excitation and emission spectra of Eu^{2+} in SrF_2 are shown in Fig. 4. It is important to note that all the samples presented in this work are shown under identical condition. The spectra clearly consist of broad excitation and emission bands centred at 332 and 416 nm, respectively. It is well known that such broad excitation and emission bands are mainly originating from the inter-configuration $4f^65d^1$–$4f^7$ allowed transition of Eu^{2+} [12,23]. The inset graph in Fig. 4 shows the emission intensity variation as a function of Eu^{2+} concentration. The maximum luminescence intensity occurred for the sample doped with 1.5 mol% and a further increase in concentration resulted in a decrease in Eu^{2+} emission intensity.

To study the energy transfer in the Eu^{2+}-Yb^{3+} couple as well as the influence of Na^+ on Yb^{3+} emission, a series of powder samples were prepared with 0.5 mol% Na^+, 1.5 mol% Eu^{2+} and various Yb^{3+} concentrations under identical conditions. In Fig. 5(A) and (B) the emission spectra for the visible region of the Eu^{2+} and NIR of the Yb^{3+} with fixed Eu^{2+} and varied Yb^{3+} concentrations are shown. Under UV excitation the PL spectra of Eu^{2+} clearly showed the broad emission band centred at 416 nm which is similar to that in the Eu^{2+} singly doped SrF_2 crystal. The NIR emission spectra that is shown in Fig. 5(B) correspond to the Yb^{3+} ions' transitions from the $^2F_{5/2}$ excited state to the $^2F_{7/2}$ ground state. The Yb^{3+} emission is strongly affected by the Na^+ impurity ions. One can see that the emission intensity of Yb^{3+} at 1 mol% (Fig. 5(B)) is relatively different from the other spectra. It consists of two narrow peaks centred at 978 and 1035 nm. With increased Yb^{3+} concentration, the shape and position of these two peaks were significantly changed. The peak at 1035 nm strongly blue shifted whereas the peak at 978 nm gradually blue shifted and broadened. The influence of Na^+ on the absorption and emission of the Yb^{3+} ion has been previously reported [17,19,22]. All these previous studies agreed that the Na^+ ions give rise to narrow and clearly resolved, small blue shifted, emission and absorption spectra of the Yb^{3+} ions. In this study, one can conclude that the Na^+ impurity ions strongly influence the Yb^{3+} spectra at low Yb^{3+} concentrations. This is because at low Yb^{3+} concentrations the Na^+ sites are abundant whereas an increase in the Yb^{3+} concentrations gradually transformed the structure to a mixture of the two cubic phases of SrF_2 and $NaYbF_4$ with fluorine interstitial sites.

From Fig. 5(A) it can be seen that the Eu^{2+} (1.5 mol%) emission ($4f^65d \rightarrow 4f^7$ transition) gradually decreased until it is almost totally
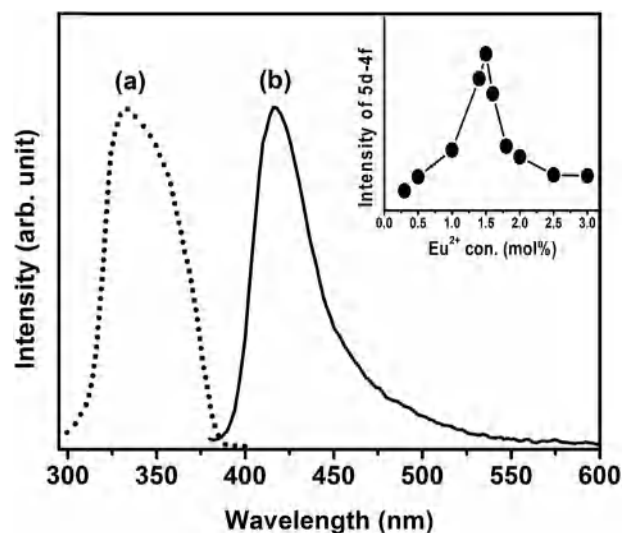

Fig. 3. Diffuse reflectance spectra of 1.5 mol% Eu^{2+} co-doped in SrF_2: 0.5 mol% Na^+ with 15 and 30 mol% Yb^{3+} ions' concentrations.

Fig. 4. Excitation spectrum (dotted line) and emission spectrum (solid line) of SrF_2:Eu^{2+} 1.5 mol% excited by 332 nm. The inset shows the Eu^{2+}:5d-4f transition's emission intensity as a function of the Eu^{2+} concentration.
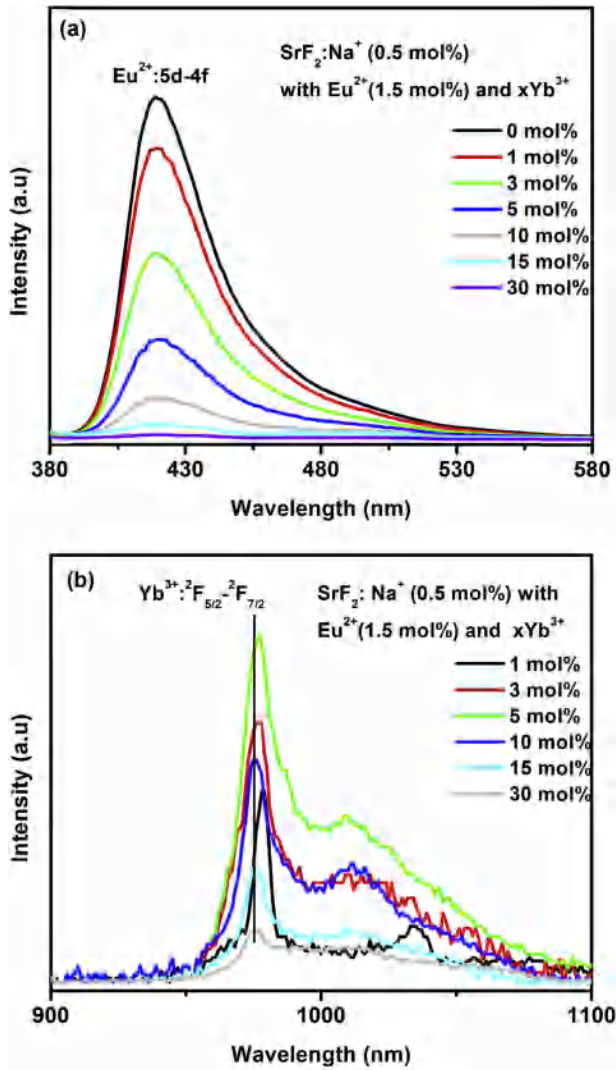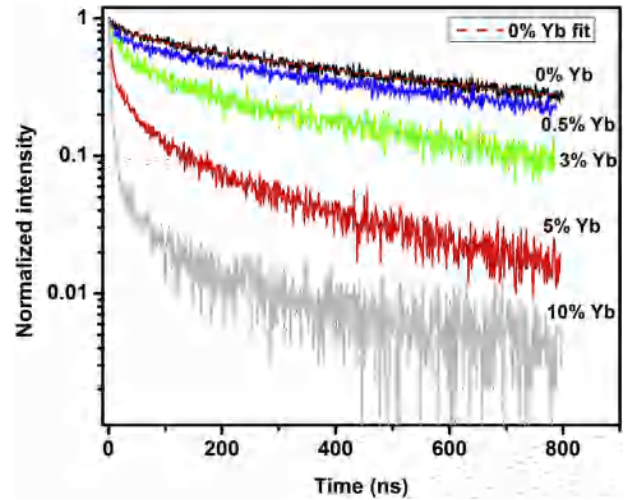
Fig. 6. Normalized decay curves of the Eu^{2+} emission at 416 nm as a function of the Yb^{3+} concentration.

Table 1
The average decay lifetime (τ (ns)) of the 5d-4f transition of Eu^{2+} (416 nm) and the Eu^{2+}-Yb^{3+} energy transfer efficiency ($\eta_{ET,x\%Yb}$).

Yb^{3+} conc. (mol%)	τ (ns)	$\eta_{ET,x\%Yb}$ (%)
0	435	0
0.5	383	12
3	243	44
5	105	76
10	47	89

Fig. 5. (a) Eu^{2+} emission intensity as a function of Yb^{3+} concentration and (b) NIR emission spectra as a function of Yb^{3+} concentration excited by a He−Cd laser system with a 325 nm excitation wavelength.

quenched at the highest Yb^{3+} concentration. On the contrary, the Yb^{3+} emissions are enhanced steadily with increased Yb^{3+} concentration (up to 5 mol%). This is shown in Fig. 5(B) where the NIR emission of Yb^{3+} are plotted with varied Yb^{3+} concentrations. The increase in the Yb^{3+} concentration resulted in a concentration quenching effect that occurred to the Yb^{3+} emissions at higher (higher than 5 mol%) concentrations. This can be attributed to the concentration quenching caused by the interactions between the nearby Yb^{3+} ions. The decrease in the Eu^{2+} emission indicates that there most likely exists an energy transfer from Eu^{2+} to Yb^{3+}.

Fig. 6 shows the decay curves of Eu^{2+}:$4f^65d^1$–$4f^7$ (416 nm) with varied Yb^{3+} concentration. The decay times of Eu^{2+} in the singly doped and co-doped samples are listed in Table 1. The decay time for the singly doped Eu^{2+} was 435 ns. This decay time was due to radiative decay from the $4f^65d^1$ (T_{2g}) level, which is well in agreement with a reported value for the decay time of Eu^{2+} emission in SrF_2 [24]. Co-doping with Yb^{3+} ion induced faster decay, which can be attributed to the energy transfer from Eu^{2+} to Yb^{3+}. An estimation of energy transfer efficiency can be obtained from $\eta_{ET,x\%Yb} = 1-\tau_x/\tau_0$ as outline in literature [25,26]. Here, τ_x and τ_0 are the corresponding average lifetimes of Eu^{2+} in the presence

and absent of Yb^{3+}, respectively. From Table 1, the energy transfer efficiency of Eu^{2+} increased gradually with an increase in the Yb^{3+} concentration. The energy transfer efficiency for the sample doped with 1.5 mol% Eu^{2+} and 10 mol% Yb^{3+} is about 89%. This shows that the Eu^{2+}-Yb^{3+} energy transfer is completed at these higher concentrations. For concentration higher than 10 mol% Yb^{3+}, the decay curves of Eu^{2+} however seem to remain constant. This might be attributed to the decrease of the Eu^{2+} lifetime less than the pulsed duration of the laser system, which was used to measure the Eu^{2+} PL decay curves. The Yb^{3+} emission was quenched due to concentration quenching at these higher concentrations. The energy transfer between Eu^{2+} and Yb^{3+} has been reported to occur through cooperative quantum cutting energy transfer [8,9]. The energy transfer based on cooperative quantum cutting has been realized in different lanthanide ion couples [8,27,28]. The quantum cutting energy transfer is based on two different models for the interaction between the donor and acceptor centers, i.e. first order energy transfer and second-order energy transfer. In the first order energy transfer, the emission spectrum of the donor should overlap with the excitation spectrum of the acceptor. In the case where the overlap between the donor's emission and acceptor's absorption spectra is absent, second-order down-conversion may become the dominant relaxation process [27]. The resonance condition occurs when the sum of the energy of the absorption transitions of the two acceptor centers approximately equals the energy of the donor's emission. The first order energy transfer can be excluded to occur in Eu^{2+}-Yb^{3+} couple, since energy overlap does not exist. Hence, the energy transfer between Eu^{2+} and Yb^{3+} couple occurred through cooperative quantum cutting energy transfer, where one Eu^{2+} photon split to excite two Yb^{3+} ions.

The total quantum efficiency of the SrF_2:Eu^{2+}, Yb^{3+} is defined as the ratio between the total number of photons emitted by Eu^{2+} to
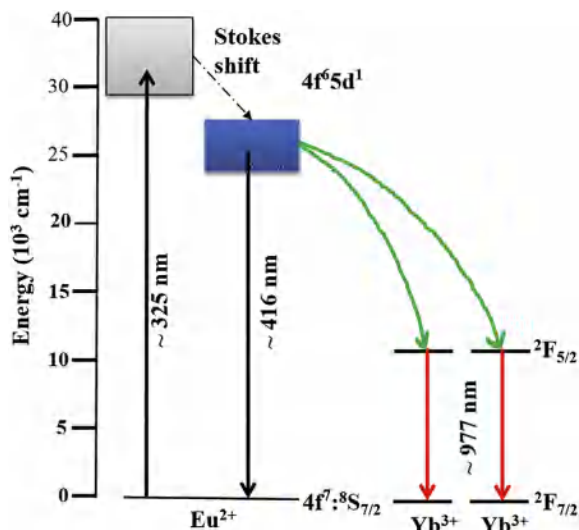
Fig. 7. Schematic energy level diagrams of Eu^{2+} and Yb^{3+} in SrF_2 and possible energy transfer process between Eu^{2+} and Yb^{3+}.

the number of the photons absorbed by Yb^{3+}, and can be calculated as a function of Yb^{3+} concentration by Ref. [29]:

$$\eta = \eta_{Eu}\left(1 - \eta_{ET,x\%Yb}\right) + 2\eta_{Yb}\,\eta_{ET,x\%Yb}$$

where η_{Eu} and η_{Yb} are the quantum efficiency of Eu^{2+} and Yb^{3+} luminescence, respectively, which are set to unity [29,30]. Considering only the Eu^{2+} energy transfer, the highest quantum efficiency, 189%, was obtained for samples co-doped with 10 mol%. However, the actual quantum efficiency is lower due to the concentration quenching and other non-radiative decay processes for Yb^{3+} or due to other quenching sites originating from material defects.

The schematic energy levels with the electronic transitions, which may be involved in the cooperative energy-transfer process between one of the Eu^{2+} ions and two of the Yb^{3+} ions in the SrF_2 crystal are shown in Fig. 7. The emission energy of the Eu^{2+}:$4f^65d^1 \rightarrow 4f7$ transition is approximately twice that of the Yb^{3+}:$^2F_{5/2} \rightarrow {}^2F_{7/2}$ transition. Upon the 325 nm excitation, Eu^{2+} ions emit at 416 nm due to the $4f^65d^1$-$4f^7$ transition, which activates two NIR photons due to the Yb^{3+}: $^2F_{5/2}$-$^2F_{7/2}$ transition. The present results suggested that Eu^{2+} can be used as an efficient sensitizer to enhance the Yb^{3+} NIR emission through a cooperative quantum cutting process.

4. Conclusion

Various Yb^{3+} ions' concentrations and Na^+ (0.5 mol%) co-doped in SrF_2:Eu^{2+} (1.5 mol%) were prepared by the co-precipitation method. XRD results showed a mixture of the two cubic phases of SrF_2 and $NaYbF_4$ at high Yb^{3+} concentrations. At low Yb^{3+} concentrations the NIR emission was strongly affected by the Na^+ substitutional sites. Cooperative energy transfer from Eu^{2+} to Yb^{3+}

ions was demonstrated. The broad emission band of Eu^{2+} ($4f^65d \rightarrow 4f^7$) leads to efficient NIR emission from Yb^{3+} through the quantum cutting process. The broad UV–Vis energy excitation photons that were efficiently converted into NIR energy photons corresponded well with the energy of the bandgap of Si. We therefore conclude that the material studied in this work might have practical application possibilities for raising the efficiency of c-Si solar cells.

References

[1] B.M. Van der Ende, L. Aarts, A. Meijerink, Phys. Chem. Chem. Phys. 11 (2009) 11081–11095.
[2] X. Huang, S. Han, W. Huang, X. Liu, Chem. Soc. Rev. 42 (2013) 173–201.
[3] Q.Y. Zhang, X.Y. Huang, Prog. Mater. Sci. 55 (2010) 353–427.
[4] B.M. Van der Ende, L. Aarts, A. Meijerink, Adv. Mater. 21 (2009) 3073–3077.
[5] T. Trupke, M.A. Green, P. Wurfel, J. Appl. Phys. 92 (2002) 1668–1674.
[6] S. Xu, W. Xu, B. Dong, X. Bai, H. Song, J. Appl. Phys. 110 (2011) 113113–113119.
[7] F. You, A.J.J. Bos, Q. Shi, S. Huang, P. Dorenbos, J. Phys. Condens. Matter 23 (2011) 215502–215508.
[8] Q. Yan, J. Ren, Y. Tong, G. Chen, J. Am. Ceram. Soc. 96 (2013) 1349–1351.
[9] J. Zhou, Y. Teng, G. Lin, X. Xu, Z. Ma, J. Qiuc, J. Electrochem. Soc. 157 (2010) B1146–B1148.
[10] Y. Teng, J. Zhou, X. Liu, S. Ye, J. Qiu, Opt. Express 18 (2010) 9671–9676.
[11] M.Y.A. Yagoub, H. C Swart, E. Coetsee, in: Proceeding of SASEC2015: Third Southern African Solar Energy Conference, 2015, pp. 471–475. Available online at: http://edas.info/web/sasec2015/program.html.
[12] M.Y.A. Yagoub, H. C Swart, L. L Noto, J.H. O'Connell, M. E Lee, E. Coetsee, J. Lumin. 156 (2014) 150–156.
[13] K.V. Ivanovskikh, V.A. Pustovarov, M. Krim, B.V. Shulgin, J. Appl. Spectrosc 72 (2005) 564–568.
[14] B.M. Van der Ende, L. Aarts, A. Meijerink, Adv. Mater 21 (2009) 3073–3077.
[15] K. Ivanovskikh, V. Pustovarov, A. Smirnov, B. Shulgin, Phys. Stat. Sol.(c) 4 (2007) 889–892.
[16] N. Kristianpoller, D. Weiss, R. Chen, Radiat. Meas 38 (2004) 719–722.
[17] L. Su, J. Xu, H. Li, W. Yang, Z. Zhao, J. Si, Y. Dong, G. Zhou, Opt. Express 30 (2005) 1003–1006.
[18] D.W. Pack, W.J. Manthey, D.S. McClure, Phys. Rev. B 40 (1989) 9930–9944.
[19] I. Nicoara, M. Stef, Eur. Phys. J. B 85 (2012) 180–186.
[20] W.J. Manthey, Phys. Rev. B 8 (1973) 4086–4098.
[21] F. Wang, Y. Han, C.S. Lim, Y. Lu, J. Wang, J. Xu, H. Chen, C. Zhang, M. Hong, X. Liu, Nat. Lett. 463 (2010) 1061–1065.
[22] L. Su, J. Xu, H. Li, L. Wen, W. Yang, Z. Zhao, J. Si, Y. Dong, G. Zhou, J. Cryst. Growth 277 (2005) 264–268.
[23] P. Dorenbos, J. Lumin 104 (2003) 239–260.
[24] Q. Luo, X. Qiao, X. Fan, J. Am. Ceram. Soc. 93 (2010) 2684–2688.
[25] J. Zhou, Z. Xia, H. You, K. Shen, M. Yang, L. Liao, J. Lumin. 135 (2013) 20–25.
[26] T. Katsumata, T. Nabae, K. Sasajima, S. Komuro, T. Morikawa, J. Electrochem. Soc. 144 (1997) L243–L245.
[27] H. Wen, P.A. Tanner, Opt. Mater 33 (2011) 1602–1606.
[28] B. Fan, C. Point, J.L. Adam, X. Zhang, X. Fan, J. Appl. Phys. 110 (2011) 113107–113114.
[29] P. Vergeer, T.J.H. Vlugt, M.H.F. Kox, M.I. den Hertog, J.P.J.M. van der Eerden, A. Meijerink, Phys. Rev. B 71 (2005) 014119–014129.
[30] Q.Y. Zhang, G.F. Yang, Appl. Phys. Lett. 91 (2007) 051903–051905.